Article citation info:
NIKONIUK M, KOZŁOWSKI M. Energy properties of a contactless power supply in PRT (Personal Rapid Transit) laboratory model. Eksploatacja i Niezawodnosc – Maintenance and Reliability 2018; 20 (1): 107–114, http://dx.doi.org/10.17531/ein.2018.1.14.

Marcin NIKONIUK
Maciej KOZŁOWSKI

ENERGY PROPERTIES OF A CONTACTLESS POWER SUPPLY IN PRT (PERSONAL RAPID TRANSIT) LABORATORY MODEL

WŁASNOŚCI ENERGETYCZNE UKŁADU ZASILANIA BEZSTYKOWEGO MODELU LABORATORYJNEGO POJAZDU PRT (PERSONAL RAPID TRANSIT)*

The article presents the results of research on the operational properties of contactless power supply system used in the PRT vehicle demonstration model, made within the framework of the ECO Mobility project. The area of transport applications of the PRT automated rail transport system is presented. Elements of the ECO Mobility PRT Drive System have been described – an inductive linear motor, dynamic contactless power supply, and supercapacitor recuperation system. Electrical performance maps of the linear motor and contactless power system were presented. Also shown was the method of their use in calculation of traction energy consumption by means of theoretical journeys. The results of the simulation calculations for the trial track were presented. The results of design calculations of the power supply parameters for the planned line of the demonstrator with real dimensions are presented.

***Keywords**: PRT, contactless power supply, simulation, assumed operating traffic conditions.*

Artykuł prezentuje wyniki badań własności eksploatacyjnych układu zasilania bezstykowego zastosowanego w modelu demonstracyjnym pojazdu PRT, wykonanym w ramach projektu ECO Mobilność. Przedstawiono obszar zastosowań transportowych systemu szynowego automatycznych środków transportu PRT. Opisano rozwiązanie układu napędowego pojazdu PRT konstrukcji ECO Mobilność – napęd za pomocą indukcyjnego silnika liniowego, zasilanie bezstykowe dynamiczne oraz układ rekuperacji z zastosowaniem superkondensatora. Zaprezentowano mapy sprawności elektrycznej silnika linowego i układu zasilania bezstykowego. Przedstawiono sposób ich wykorzystania w obliczeniach zużycia energii trakcyjnej metodą przejazdów teoretycznych. Przedstawiono wyniki obliczeń symulacyjnych dla toru próbnego w skali. Przedstawiono wyniki obliczeń projektowych parametrów układu zasilania dla planowanej linii demonstratora o wymiarach rzeczywistych.

***Słowa kluczowe**: PRT, układ zasilania bezstykowego, symulacja, zakładane eksploatacyjne warunki ruchu.*

1. Introduction

Transportation solutions using PRT (Personal Rapid Transit) vehicles are not new [1]. The PRT is a mode of automatic rail transport. PRT vehicles usually run on rubber-tired wheels at special track systems [26]. Also in Poland, PRT transport applications have been subject to exhaustive analyses [5]. At present, however, there has been a renewed interest in such modes of transport, due to the concept of "pod car", which is the idea of extending the use of this type of automatic rail vehicle to public circuits [27]. Introduction of this concept can be based on two different levels of motion control automatics. At the lower level, usually designated Level 3 [29], vehicles move on separate lanes of public roads called "virtual roads" due to the need to build a special V2I communication infrastructure and communication system [10]. At the highest level, marked Level 5, vehicles should move as autonomous vehicles. PRT vehicles moving in line with the idea of "pod car" also on public roads will become part of automated transport networks (ATN) in urban areas [8]. In the future, vehicles of this type will be the synthesis of an automatic rail and wheel vehicle. In dense areas with heavy traffic, they will be able to navigate the dedicated tracks built specifically for them so that traffic infrastructure can be used in suburban areas with low traffic.

This article is devoted to the description of the power supply used in the "Polish" PRT version, made as a physical model in scale within the framework of the ECO Mobility project. This project has not yet been implemented for transport applications but has nevertheless been tested on a test track for scale vehicles. A fragment of track in scale was recently presented at the Hannover Fair at the SciTech Poland "scientific" Polish stand [7, 28].

The already mentioned power supply is a contactless, dynamic power system, which means that it can deliver energy to the vehicle in motion as opposed to stationary systems where energy is delivered only when the vehicle is stationary. The drive motor is a linear induction motor. This system solution illustrates one of the many possibilities that can be applied to the driving and powering of this type of vehicle. The power supply can also be made as a contact one with power points at parking places. Propulsion motors can be made as brushless, induction and wheeled or as central units. On the other hand, the contactless power supply has the advantage of being a safe system [23, 30]. The supply energy is transmitted inductively from the primary winding distributed along the track - similarly to the third rail in the metro. The fundamental difference between the contact supply by means of the third rail and the contactless induction is that the contact rail "power" is isolated and thus safe.

(*) Tekst artykułu w polskiej wersji językowej dostępny w elektronicznym wydaniu kwartalnika na stronie ***www.ein.org.pl***

2. Power Transmission System for PRT with contactless power supply, linear motor, and supercapacitor

The layout of the PRT drive system with the contactless power supply, the linear motor and the supercapacitor is shown in Fig. 1, where the following are marked:

– stationary part - traction substation: SE - electricity grid, TS network transformer, PS - diode mains rectifier, PR - resonant converter, KR1 - resonant circuit capacitors on the primary side, TD - matching transformer
– vehicle part: contactless power supply (CET), SZ – primary winding of the contactless energy transfer system, UW - secondary winding of the non-contact energy transfer system, KR2 – resonant circuit capacitors on the secondary side, PD – diode rectifier, FN – drive inverter, PM – bi-directional converter for energy storage and brake resistor converter, SC – supercapacitor tray, RH – braking resistor, linear induction motor (SIL)

Fig. shows a diagram of the energy increments that can be associated with separate circuits during vehicle movement. In addition, it was assumed that:

- The energy of the CET transformer is the electrical energy of a single-phase sinusoidal non-distorted 50 kHz transformer. The increments of this type of energy are indicated by the following symbols: dE_Z – CET primary power supply, dE_{CET} – CET secondary site, dE_{CS} – supercapacitor discharge, dE_{DC} – supercapacitor charge, ΔE_{CET} – CET system losses, ΔE_{CET} – supercapacitor losses.
- The energy supplying the motor is the electric current of the three-phase sinusoidal variable non-deformed variable frequency controlled by the inverter. Increments of this type of energy are denoted by: dE_{conv} - motor power, dE_R - recuperation, ΔE_{SIL} - engine loss, ΔE_R - recuperation.

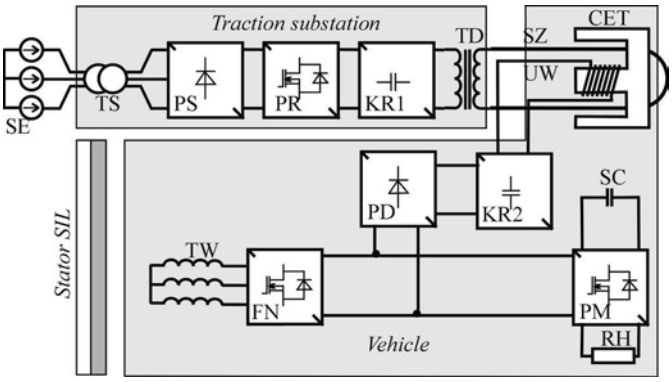

Fig. 1. Block diagram of the power supply – stationary and vehicle

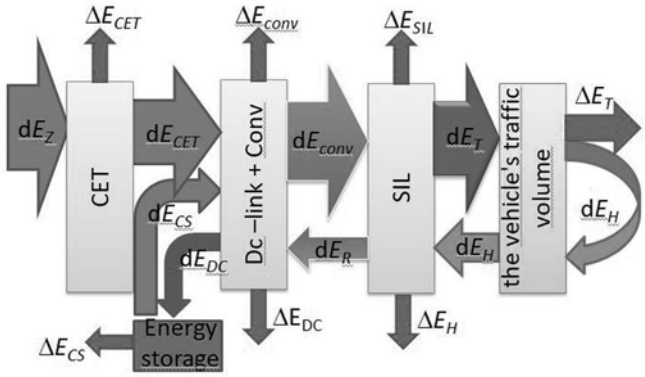

Fig. 2. Diagram of Power Transmission System for the PRT vehicle

- Propulsion energy is a form of mechanical energy. Energy increments are: dE_T - traction, dE_H - kinetic, ΔE_T - mechanical losses.

Fig. 3 presents a 1:4 physical model of PRT vehicle at the laboratory stand for the laboratory study of the power supply and motion control at the Faculty of Transport. The vehicle shown on the picture is on the crossover. On the side of the vehicle, there is a CET transformer with an open magnetic E-shaped circuit. The magnetic circuit is open so that the vehicle can freely exit the loop of the primary winding. The primary winding section is visible behind the vehicle. The vehicle travels the road section on the crossover in the power mode by superconductor energy storage.

Fig. 3. Physical model of a PRT vehicle in a laboratory station

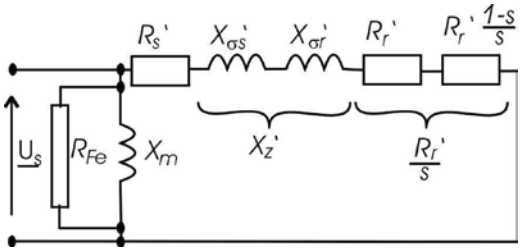

Fig. 4. Simplified peripheral circuit diagram describing the linear motor model adopted for the calculation

3. Model of linear induction motor

The energy characteristics of the steady-state drive system components can be described by efficiency, power factor and power loss as follows:

$$\eta = \frac{P_m}{P_c} \tag{1}$$

$$\cos\phi = \frac{P_c}{\sqrt{P_c^2 + Q_c^2}} \tag{2}$$

$$P_c = P_m + \Delta P \tag{3}$$

where: P_m – power on the shaft, P_c – total active power, ΔP – power losses, Q_c – reactive power.

The mechanical power of the linear motor can also be defined as the product of force and velocity:

$$P_m = F_{lin} v_{lin} \tag{4}$$

The theoretical description of the above relationships has been applied to the peripheral model of the simplest motor, known from the static modelling of the rotary engine operating state for sinusoidally variable non-distorted current supply conditions. The diagram of electrical circuit of the model substitute is shown in Fig. 4. The parameters listed are as follows: R_s - primary winding resistance, R_r - secondary winding resistance, X_z - secondary substitution reactance (consisting of scattering and stator and rotor reactances), R_{FE} - replacement resistance in iron (for vortex currents and hysteresis), X_m - magnetization reactance. Index ' means the conversion of the value of the secondary side parameter to the value of the primary side. The use of such a simple model was determined through its usefulness, understood here as the ability to obtain a sufficiently small divergence in the description of the traction-energy characteristics of the engine used in the propulsion system at the laboratory. However, it should be noted that the linear motor (in contrast to the rotary motor) has an open magnetic circuit. Marginal and edge parasitic phenomena are very important in linear motors, which can be omitted in rotary motors. The magnetic gap of the linear motor is much wider than the gap in the rotary engine. The effect of these phenomena is the reduction of the efficiency of linear induction motors and increase in the demand for reactive power to produce magnetic flux. The mathematical model of linear induction motor describing these additional phenomena is a complex process which has been found in many theoretical papers [20], also in the area of control theory [2, 24, 11].

For the accepted substitution scheme, it is possible to formulate the following set of formulas:

a) Total active power consists of rotor electromagnetic power and power loss in the iron:

$$P_c = P_m + \Delta P = F_l V_s + pm\frac{U_s^{\,2}}{R_{Fe}} \tag{4}$$

b) Reactive power is charged to the formation of the magnetizing stream and diffusion streams:

$$Q_c = \frac{sF_l V_s}{s_K} + pm\frac{U_s^{\,2}}{X_m} \tag{5}$$

c) Strength is a slip function described by the Kloss formula:

$$F_l = \frac{2F_K}{\frac{s_K}{s} + \frac{s}{s_K}} = \frac{2F_K s_K s}{\left(s_K^{\,2} + s^2\right)} \tag{6}$$

where: V_s – synchronous linear speed, m – number of phases, p – number of poles, U_s – stator voltage. F_K – critical power, s_K – critical slip, s - slip

For the accepted method of describing the active and reactive power, the determination of efficiency (1) and power factor (2) can be reduced to:

$$\eta = \frac{V_l}{V_s + m\frac{U_s^{\,2}}{F_l R_{Fe}}} \tag{7}$$

$$\cos\phi = \frac{F_l V_s + m\frac{U_s^{\,2}}{R_{Fe}}}{\sqrt{\left(F_l V_s + m\frac{U_s^{\,2}}{R_{Fe}}\right)^2 + \left(\frac{sF_l V_s}{s_K} + m\frac{U_s^{\,2}}{X_{mi}}\right)^2}} \tag{8}$$

4. Map of linear induction motor model efficiency

Table 1 shows the linear induction motor ratings of a 1:4 vehicle [12, 25]. Table 2 shows the variation of the parameters for the change in the nominal width of the air gap in a permissible construction range of 2-4 mm. Parameters of the peripheral motor model were identified by analysing the waveforms of the theoretical and laboratory-measured characteristics. This was done using the least distance method. The calculated parameters are presented in Table 3. The theoretical characteristics obtained are shown in Fig. 5: a) mechanical, b) efficiency, c) power factor.

Table 1. SIL rated characteristics

Parameter	Symbol	Unit	Value
Length of inductor	L	m	0,27
Number of pairs of poles	p	-	3
Number of phases	m	-	3
Rated gap	g_m	mm	3
Supply voltage	U_1	V	230
Rated frequency	f_n	Hz	45
Rated linear speed	V_{ln}	[m/s]	3,375
Rated power	P_{cn}	W	433
Active power	P_{1n}	W	966
Apparent power	S_{1n}	[VA]	7250

Table 2. Parameters of continuous motor operation in conditions of changing the length of the air gap in the range of 2-4 mm.

Parameter	Symbol	Unit	2	2,5	3	3,5	4,0
Slip	s_n	-	0,143	0,160	0,167	0,180	0,1901
Linear speed	V_{ln}	[m/s]	3,470	3,402	3,375	3,32	3,28
Continuous force	F_{cn}	[N]	166	148	128	116	103
Power on the shaft	P_{cn}	[W]	575	504	433	385	338
Active power	P_{1n}	[W]	1148	1053	966	1006	1039
Apparent power	S_{1n}	[VA]	7250	7250	7250	7250	7250
Efficiency	η_N	-	0,50	0,48	0,448	0,38	0,32
Power factor	$\cos\varphi_N$	-	0,158	0,146	0,133	0,14	0,14
Energy factor	$\eta_N * \cos\varphi_N$	-	0,079	0,070	0,060	0,053	0,047

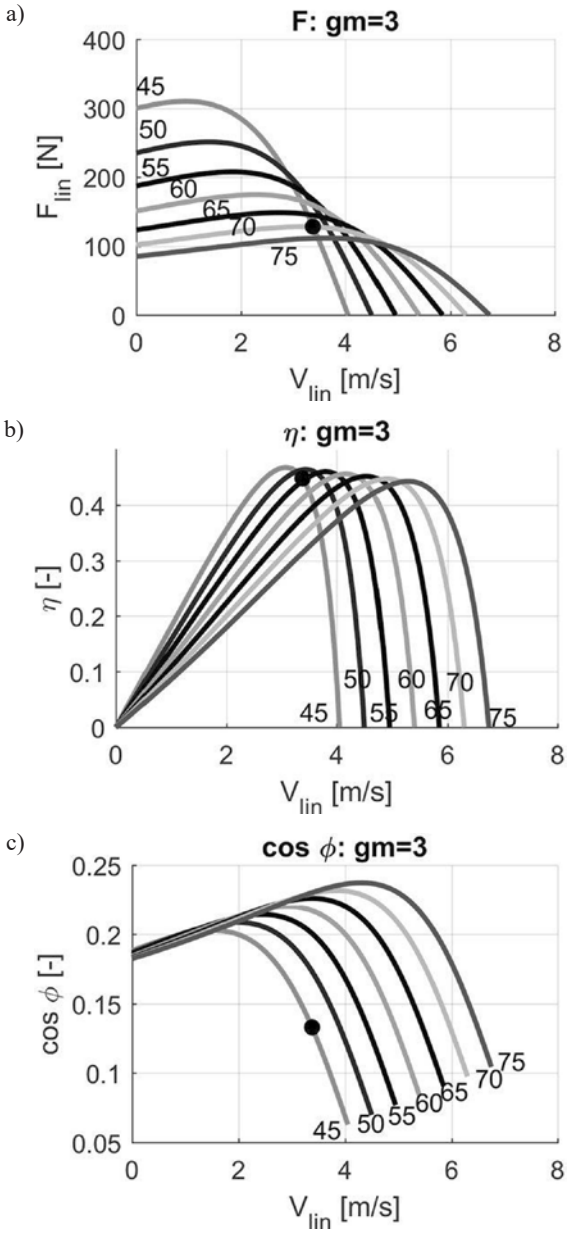

Fig. 5. SIL natural characteristics: mechanical, efficiency (η) and power factor (cos ϕ) for different values of supply voltage frequency

Table 3. Parameters of the replacement scheme for different air gap widths

Symbol	Unit	2	2,5	3	3,5	4,0
X_Z'	[Ω]	151	170	189	213	235
R_r'	[Ω]	97	121	146	174	207
X_m	[Ω]	68	68	67	67	66
R_{Fe}	[Ω]	998	1051	1066	888	767

Fig. 6 shows a map of the efficiency and power factor of the motor for the gap width of 3 mm. The parameters listed in Table 3 provide maps for the remaining slot widths.

5. Model of contactless power supply

The basic element of the contactless power supply system is the high frequency CET transformer, whose primary and secondary windings are maintained in the resonant state - using additional capacitors

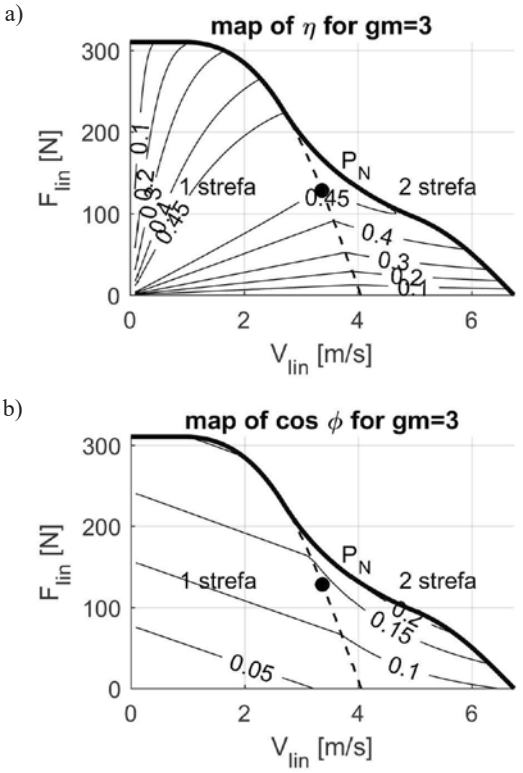

Fig. 6. SIL performance and power factor charts for the laboratory drive for a slot width of 3 mm

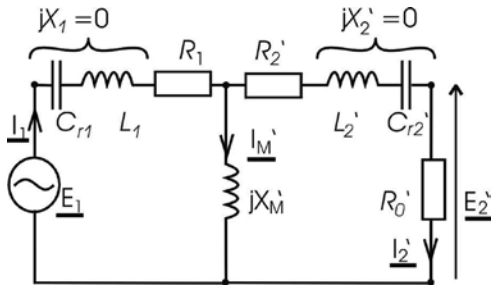

Fig. 7. Diagram of substitution circuit of CET transformer

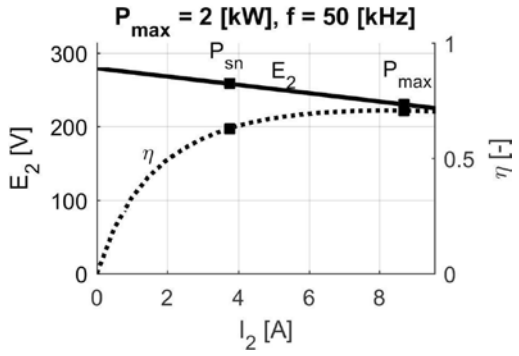

Fig. 8. Contactless power supply diagrams: external $E_2(I_2)$ and efficiency $\eta(I_2)$

(X1 = X2 = 0) [3, 9, 13, 14, 22]. The circuit diagram used to describe the steady-state condition of the sine wave voltage supply [4, 21] is shown in Fig. 7.

Marked: R_1 – primary winding resistance, R_2' – secondary winding resistance reduced to primary side, R_0' – receiver resistance reduced to primary side, L_1 – inductance of primary winding, L_2' – inductance

of secondary winding reduced to primary side, C_{r1} – capacitance of the primary compensation capacitor, C_{r2}' – capacitance of the secondary compensation capacitor reduced to primary side, X_M' – magnetic coupling reactance reduced to primary side, X_1 – replacement reactance of serial connection $L_1 - C_{r1}$, X_2' – replacement reactance of serial connection $L_2 - C_{r2}$ reduced to primary side, I_1 – primary current, I_2' – secondary current reduced to primary side, E_1 – primary power supply voltage, E_2' – receiver voltage reduced to primary side.

The power allocated at the receiver is determined by the formula:

$$P_{out} = (I_2')^2 R_0' \tag{9}$$

The power output from the source is the sum of the power output at all resistances of the circuit:

$$P_{in} = P_{out} + \Delta P = I_1^2 R_1 + (I_2')^2 \left(R_2' + R_0'\right) \tag{10}$$

Electrical efficiency is defined by the formula:

$$\eta = \frac{P_{out}}{P_{in}} = \frac{(I_2')^2 R_0'}{(I_1)^2 R_1 + (I_2')^2 \left(R_2' + R_0'\right)} \tag{11}$$

The reactive power of the system is only taken to produce a magnetizing stream:

$$Q_{in} = (I_M')^2 X_M' \tag{12}$$

The power factor is defined by the formula:

$$cos\varphi = \frac{P_{in}}{S_{in}} = \frac{(I_1)^2 R_1 + (I_2')^2 \left(R_2' + R_0'\right)}{\sqrt{\left((I_1)^2 R_1 + (I_2')^2 \left(R_2' + R_0'\right)\right)^2 + \left((I_M')^2 X_M'\right)^2}} \tag{13}$$

The output voltage of the contactless power system is determined by the formula:

$$\underline{E_0} = \underline{E_2}' + \underline{Z_w}' \underline{I_2}' \tag{14}$$

where: $\underline{E_0}$ – is idle voltage, $\underline{Z_w}$' – is internal impedance of the power supply.

The formula for external characteristic describes the cosine pattern, which after transformations takes the following form:

$$E_0^2 = (E_2')^2 + (Z_w' I_2')^2 + 2(E_2')(Z_w' I_2')\cos\psi_w \tag{15}$$

where additionally: ψ_W – phase angle between current and voltage in internal impedance.

Based on the calculated design calculations and measurements of CET transformer parameters for the vehicle power supply, the following parameters of the peripheral model were adopted: $M = 5 \cdot 10^{-6}$ H, $R_1 = 18 \cdot 10^{-3}$ Ω, $R_2 = 20 \cdot 10^{-3}$ Ω, $\upsilon = 1/18$, $f = 50 \cdot 10^3$Hz [19]. The required maximum power of the motor $P_{max} = 2 \cdot 10^3$ W is developed at a voltage of $U_s = 230$ V, under voltage conditions of $E_1 = 280/18$ V. Fig. 8 shows the characteristics of a contactless power supply system: external $E_2(I_2)$ designated E_2 (converted to secondary side) and efficiency $\eta(I_2)$ designated η. Two selected work points are indicated in the drawing: P_{sn} – the load point of the system with the active power corresponding to the rated operating conditions of the motor with a 3mm magnetic slot (966 W – table 1) and P_{max} – the maximum load point with the active power.

6. Theoretical analysis of the energy properties of the power supply system for the assumed operating conditions of the laboratory vehicle.

The starting point for the analysis of the energy consumption of the vehicle drive system is the analysis of demand for power (energy) mechanical, popularly known as traction power. The diagram of the applied traction power calculation method is shown in Fig. 9 [18], where: Speed – predetermined instantaneous speed, Route – predetermined path and path profile, P_K – increase in kinetic energy over time, P_V – power to overcome aerodynamic motion resistance, $F_R \cdot v_{lin}$ – power to overcome the forces of additional resistance (corners). In the presented method the power component of the motion resistance is the function of the arc radius R and the velocity v_{lin}, determined interpolatively on the basis of the results obtained through simulation [15] using the vehicle dynamics models [15, 16]. Fig. 10 shows a diagram of a laboratory track, where the symbols H mark the stops, K – switches, L – track connections. Fig. 11 depicts the interstitial distribution travel speed in the H4 – H2 fragment (as a function of the road), determined from the solutions of the computational model of the structure shown in Fig. 9. The dashed line indicates speed limits on the corners. The limitations of traction forces in the form of the characteristics shown in Fig. 6 and the influence of the forces of motion resistance (basic from speed and additional curvature of the trajectory) are taken into account in determining the course of speed. Fig. 12 shows the driving force of the SIL motor (as a function of time) on the analysed road segment.

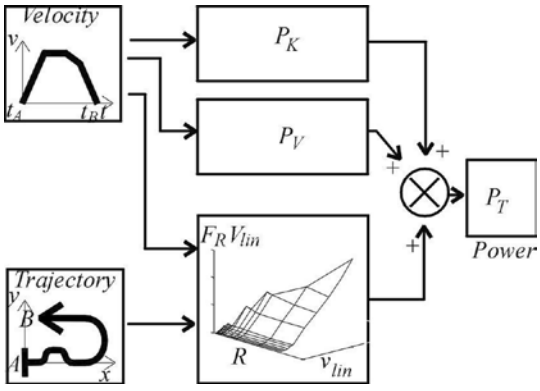

Fig. 9. Diagram of determination of traction power

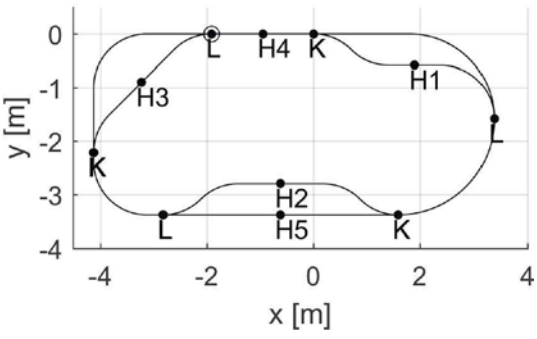

Fig. 10. Track diagram for occupational tests (Faculty of Transport lab)

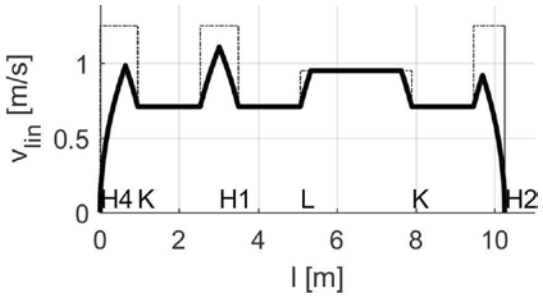

Fig. 11. Distribution of speed as a function of road while passing on the interstitial section of road H4-H5

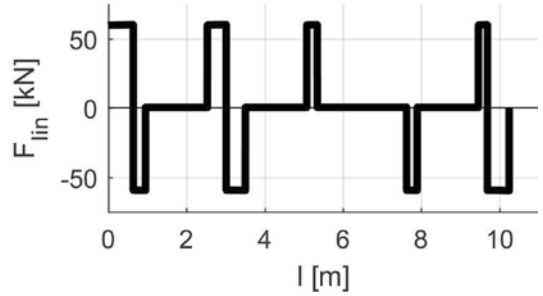

Fig. 12. Waveform of driving force SIL as a function of time on the section of road H4-H5

The above forces and velocities are the basis for determining the power supply of the SIL motor. The calculation takes into account the efficiency of the motor function of the map shown in Fig. 6. The calculation of power output is shown in Fig. 13. The graphs are marked: 1 - the instantaneous power of SIL motor, - 2 the instantaneous power to be delivered from the PD rectifier (fig.1) when a supercapacitor is used in the system. The negative values of power in diagram 1 correspond to the possibility of applying the electric braking of the vehicle. According to the diagram of Fig. 2, the recuperation process is based on the accumulation of braking energy in the supercapacitor and the equalization of the starting power. The calculations take into account the share of the energy loss in the supercapacitor system.

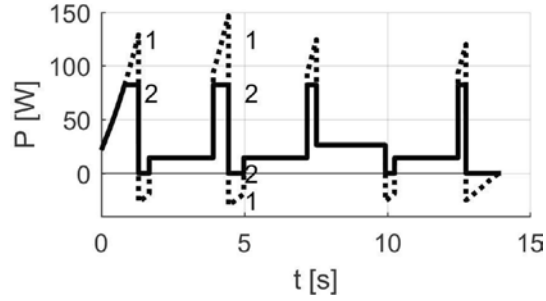

Fig. 13. Power of the SIL power supply. Diagrams are: 1 - without energy storage on the vehicle, 2 - in a system with supercapacitor

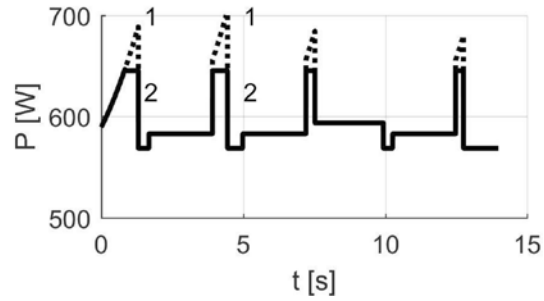

Fig. 14. Power cycle of the laboratory vehicle power supply on the CET contactless power supply terminals. Diagrams are marked: 1 - without energy storage on the vehicle, 2 - in the system with supercapacitor

7. Theoretical analysis of the energy properties of the power supply system for the assumed operating conditions of the vehicle with actual dimensions.

One of the locations considered for the construction of the PRT is the city of Rzeszow. At this stage of the discussions, the type of electric motors used for the drive and the way the vehicle will be powered for that location are not yet determined. However, traction calculations show that a train of actual size and a max. speed of 50 km/h will require a drive with a nominal capacity of approx. 16 kW. Brushless motors located in the wheels of a vehicle which are already used in the car's ECO pre-processor, can be used to implement the drive, for example. The power loss maps of this engine are shown in publication [17]. Equally good is the use of 5-phase induction motors in wheel hubs. This type of engine dedicated to automotive applications was recently presented by HCP at the Hannover Fair. In the already completed ECO Mobility project, a linear induction motor design was implemented [12]. The performance map of this motor is shown in Fig. 15. Fig. 16 shows the external characteristics and performance characteristics of the contactless power system designed in this solution. Fig. 17 shows a diagram of the track line of one of the route sections in the planned location. Fig. 18 shows the driving speeds of the forcing drive - minimum time at this section of the road. Speed limits result from both the limits of the maximum permissible axial acceleration on the curvature of the tracks and the speed limits for direct driving conditions. The exponential acceleration and motion delays result from the possibility of obtaining maximum traction forces (described in the form of the F-V relation in Fig. 15). Fig. 19 shows the course of traction forces on the analysed section of the road, and Fig. 20 shows the power flow patterns. In this figure, the waveforms are shown in two possible variants of the vehicle power supply solution: black diagram - waveform without additional power source, blue - with supercapacitor system for braking energy return (recupera-

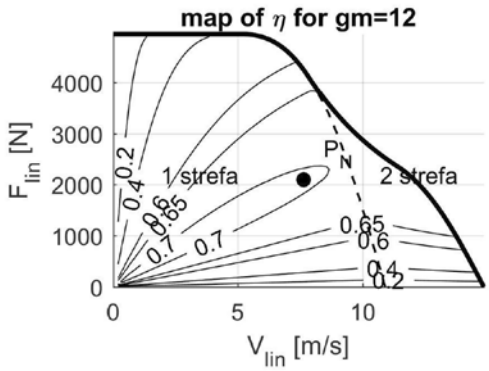

Fig. 15. SIL performance charts for vehicles with actual dimensions at a gap width of 12 mm

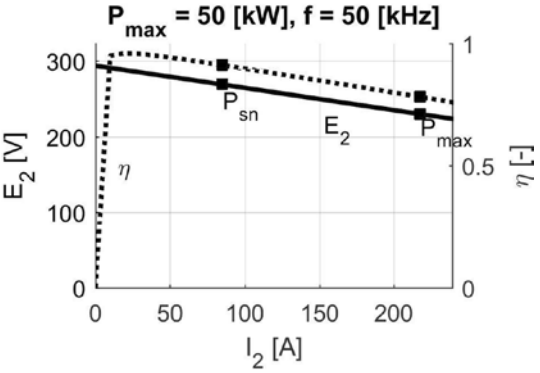

Fig. 16. Contactless power supply diagrams: external E2(I2) and efficiency η(I2)

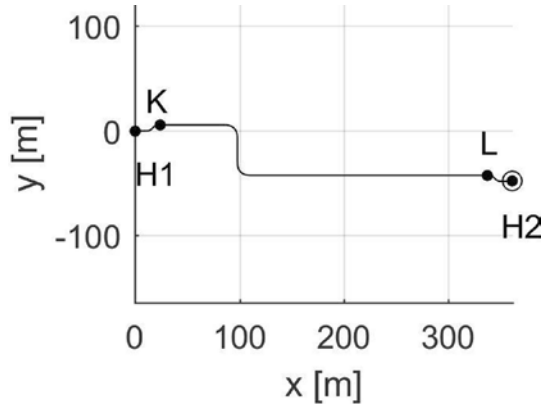

Fig. 17. Diagram of the track line of the first section of the route for the planned location of the PRT track in Rzeszow

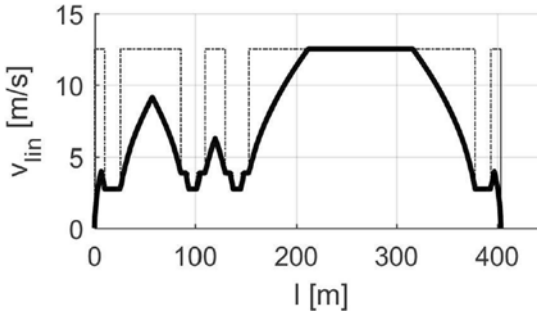

Fig. 18. Distribution of speed as a function of road during the passage of the section in the city of Rzeszow

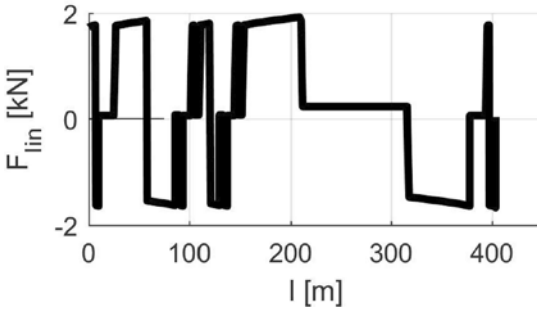

Fig. 19. Distribution of SIL driving force as a function of the road section of the city of Rzeszow

tion system). Fig. 21 shows power draws on the primary source side of the CET transformer. When using an energy recovery system, the maximum input power of the system is approximately 12 kW.

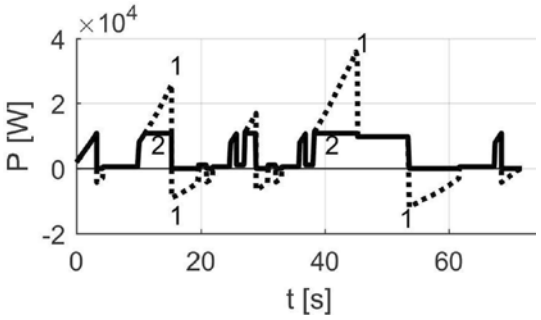

Fig. 20. Power step at the output of the PD rectifier (fig. 1). Diagrams are: 1 - without energy storage on the vehicle, 2 - in the system with supercapacitor

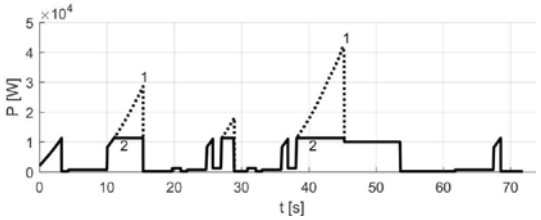

Fig. 21. The power of the vehicle power supply on the terminals of the contactless power supply CET for the section in the city of Rzeszow. Diagrams are: 1 - without energy storage on the vehicle, 2 - in the system with supercapacitor

8. Conclusions

The conducted analysis of the PRT drive and the laboratory tests of vehicles on a test scale showed that dynamic contactless power may be considered as one of the methods of supplying electricity to vehicles of actual size. This type of power supply is ideal for small vehicles moving in urban infrastructure, where safety considerations are particularly important. Results of analyses and studies also show that low power linear induction motors are characterized by low values of energy coefficients (both efficiency and power factor). The 16kW engine designed for the vehicle with actual dimensions is also characterized by poorer operating conditions than rotary motors. The use of linear motors also excludes the possibility of moving this PRT vehicle on public roads intended for wheeled vehicles. For this reason, the second generation of currently-developed PRT vehicles will be equipped with rotary motors. These vehicles will be able to have a contactless power supply system as a rail system, supplemented by electrochemical energy storage on board the vehicle. During the rail traffic, the contactless power supply system will provide the energy required to track the path and the energy to charge the electrochemical battery, which will be a source of power during the period of moving on the public road.

References

1. Anderson J E. A Review of the State of the Art of Personal Rapid Transit. Journal of Advanced Transportation 2000; 34(1): 3-29, https//doi.org/10.1002/atr.5670340103.
2. Berrin S, Vedat M. Karsli. Direct Thrust Controlled Linear Induction Motor Including End Effect. 13th International Power Electronics and Motion Control Conference 2008.
3. Böttigheimer M, Parspour N, Zimmer M, Lusiewicz A, Design of a Contactless Energy Transfer System for an Electric Vehicle, PCIM Europe 2016; ISBN 978-3-8007-4186-1
4. Boys J, Kazmierkowski M P, Lomonova E, Madawala U, Covic G. Special Section on "Contactless Energy Transfer Systems " IEEE Transactions on Industrial Electronics 2013; 60(1): 212, https://doi.org/10.1109/TIE.2012.2203489.
5. Chormański W. Systemy transportowe PRT. Wydawnictwa Komunikacji i Lacznosci - Transport and Communication Publishers 2015: 38.
6. Codziennypoznan.pl: Powstanie innowacyjny elektryczny samochód dostawczy z silnikiem opracowanym w Zakładach Cegielskiego w Poznaniu, http://www.codziennypoznan.pl/artykul/2017-04-27/powstanie-innowacyjny-elekt ryczny-samochod-dostawczy-z-silnikiem-opracowanym-w-zakladach-cegielskiego-w-poznaniu [2017-07-13]
7. Dziennik naukowy.pl. Polskie technologie i wynalazki na targach Hannover Messe 2017 http://dzienniknaukowy.pl/nauka-w-polsce/olskie-

technologie-hannover-messe- 2017/ [2017-07-13]
8. Furman B, Fabian L, Ellis S, Muller P, Swenson R. Automated Transit Networks (ATN): A Review of the State of the Industry and Prospects for the Future, MTI Report 2014
9. Judek S., Karwowski K.: Contactless electrical energy transfer system via magnetically coupled air coils. Gdańsk: Wyd. Politechniki Gdańskiej, 2013, ISBN 978-83-7348-501-3
10. Jurgen R K. V2V/V2I Communications for Improved Road Safety and Efficiency, SAE International. Product Code of PT-154 2012, ISBN of 978-0-7680-7725-4, https://doi.org/10.4271/PT-154.
11. Kamiński B, Nikoniuk M, Drążikowski Ł. A concept of propulsion and power supply systems for PRT vehicles. Archiwum Transportu - Archives of Transport 2013; 27(3-4): 81-93.
12. Kamiński G., Przyborowski W., Staszewski P., Biernat A., Kupiec E., Design and testing of Laboratory Model of Linea Induction Motor for Automation Personal Urban Transport PRT, Przeglad Elektrotechniczny -Electrical Review 2017; 93(3): 276-283.
13. Kazmierkowski M P, Miskiewicz R M, Moradewicz A J. Inductive coupled contactless energy transfer systems - a review. Selected Problems of Electrical Engineering and Electronics (WZEE) 2015.
14. Kazmierkowski M P, Moradewicz A J, Duarte J, Lomonova E, Sonntag Ch. Chapter 35 "Contactless Energy Transfer" in The industrial Electronics Handbook, Part II: Power Electronics and Motor Drives, Second Edition, Edited by B. M. Wilamowski, J. David Irvin, CRC Press 2011.
15. Kozłowski M, Choromański W, Kowara J. Analysis of dynamic properties of the PRT vehicle-track system. Bulletin of the polish academy of sciences, Technical sciences 2015; 63(3): 799-806, https://doi.org/10.1515/bpasts-2015-0091.
16. Kozłowski M, Choromański W, Kowara J. Parametric sensitivity analysis of ATN-PRT vehicle (automated transit network - personal rapid transit). Journal of Vibroengineering 2015; 17(3): 1436 1451
17. Kozłowski M, Tomczuk K, Szczypior J. Methodology of determining basic technical parameters of electric-drive car, Przeglad Elektrotechniczny - Electrical Review 2011; 87(10): 299-304.
18. Kozłowski M. Simulation method for determining traction power of ATN - PRT (Automated Transit Network - Personal Rapid Transit) vehicle, Transport 2016; ISSN 1648-4142.
19. Krawczyk Z, Nikoniuk M, Starzyński J, Chaber B, Kamiński B. A prototype transformer for inductive contactless energy transfer system: numerical models verified by measurement. Przegląd Elektrotechniczny - Electrical Review 2014; 90(5): 56-60.
20. Lu G, Li Q, Liu Z, Fan Y, Li G. The Analytical Calculation of the Thrust and Normal Force and Force Analyses for Linear Induction Motor, ICSP 2008; Proceedings
21. Mecke R, Rathage C. High frequency resonant converter for contactless energy transmission over large air gap. PESC iEEE 2004; 1737-1743.
22. Moradewicz A J, Kazmierkowski M P. High efficiency contactless energy transfer system with power electronic resonant converter. Bulletin Of The Polish Academy of Sciences, Technical Sciences 2009; 57(4): 375-381, https://doi.org/10.2478/v10175-010-0141-0.
23. Nam P. Suh . Dong Ho Cho (Editors): The On-line Electric Vehicle. Wireless Electric Ground Transportation Systems. Springer 2017. ISBN 978-3-319-51182-5
24. Nikoniuk M., Kamiński B., Yaremoff O.: Zagadnienia regulacji sił ciągu i prędkości silnika indukcyjnego liniowego. rozdział 6.9, w: Ekomobilność. Innowacyjne i ekologiczne środki transportu / Choromański Włodzimierz (red.), Wydawnictwa Komunikacji i Lacznosci - Transport and Communication Publishers 2015, 1: 160-179.
25. Nikoniuk M., Kozłowski M., Model strat mocy układu napędu pojazdu PRT (Personal Rapid Transit), Prace Naukowe Politechniki Warszawskiej. Seria Transport. OWPW 2016; 112: 301-311,
26. Personal Rapid Transit. Website from Wikipedia: http://en.wikipedia.org/wiki/Personal_rapid_transit, [2017-07-13]
27. Podcar city & advanced transit conference 2017. Smart Cities, Smart Transportation, Smart Energy. Las Vegas USAr 8-10 November 2017. Website at: http://www.advancedtransit.org/library/news/podcar-city-advanced-transit-con ference-2017/ [2017-07-13]
28. Politechnika Warszawska Badania i Nauka, Reprezentanci Politechniki Warszawskiej na targach Hannover Messe, Web Site: 2017 https://www.pw.edu.pl/Badania-i-nauka/Aktualnosci/Reprezentanci-Politechniki -Warszawskiej-na-targach-Hannover-Messe-2017 [2017-07-13]
29. Radovanovic D, Muoio D. This is what the evolution of self-driving cars looks like, Finance on line, Business Insider, http://www.businessinsider.com/what-are-the-different-levels-of-driverless-cars-2016-10?IR=T/#-1 [2017-07-13]
30. Worek C. Bezstykowy przesył energii elektrycznej oparty o szeregowo-równoległe układy rezonansowe http://ptetis.agh.edu.pl/CWorek.pdf. 2013 [2017-07-13]

Marcin NIKONIUK
Maciej KOZŁOWSKI
Department of Information Technology and Mechatronics in Transport
Warsaw University of Technology,
Faculty of Transport,
ul. Koszykowa 75, 00-662 Warszawa, Poland

Emails: marcin.nikoniuk@wt.pw.edu.pl, mkozlo@wt.pw.edu.pl